ELSEVIER

Journal of Alloys and Compounds 444–445 (2007) 621–633

Journal of ALLOYS AND COMPOUNDS

www.elsevier.com/locate/jallcom

Molecular magnetism in neptunyl (+1, +2) complexes: ^{237}Np-Mössbauer and magnetic study☆

A. Nakamura [a,*], M. Nakada [a], T. Nakamoto [a,1], T. Kitazawa [b], M. Takeda [b]

[a] *Advanced Science Research Center, Japan Atomic Energy Agency (JAEA), Tokai, Ibaraki 319-1195, Japan*
[b] *Department of Chemistry, Faculty of Science, Toho University, Funabashi, Chiba 274-8510, Japan*

Received 7 September 2006; received in revised form 13 December 2006; accepted 17 December 2006
Available online 21 December 2006

Abstract

The results of ^{237}Np-Mössbauer and magnetic study on neptunyl (+1, +2) (Np(V, VI); $5f^{2,1}$) complexes are discussed, focusing on their unique neptunyl $(O{=}Np(V, VI){=}O)^{+1,+2}$-based low-dimensional (low-D) molecular magnetism in correlation with their structural details (the individual 'nyl'-based uniaxial molecular structure, its dimensionality extended by the so-called 'cation–cation bond' (CCB), and their differences between the neptunyls (+1) and (+2), etc.). For this purpose, first, the X-ray diffraction (XRD) and ^{237}Np-Mössbauer data on their basic structural and electronic (hyperfine electric-quadrupole and magnetic) properties are described. On this basis, magnetic properties of over-10 oxo-neptunyl (+1) complexes are discussed and summarized, revealing several salient structure–magnetic property correlations in these systems such as the crucial role of 2D-CCB network structure for the onset of long-range magnetic order. As for the neptunyl (+2) complexes for which magnetic data are very sparse, the results of our most-recent study on the three systems, an oxo-trinitrato **1** $NH_4[NpO_2(NO_3)_2]$ and two pyridine (py = C_5H_5N) complexes, **2** $NpO_2(acac)_2py$ (acac = $C_5H_7O_2^-$) and **3** $NpO_2(NO_3)_2byp$ (bpy (bipyridine) = $C_{10}H_8N_2$), are presented. Here, due to the higher (+2) neptunyl valence state, the CCB is not generally formed, and all these three are nominally the 0D non-CCB systems. Oxo-**1** was found to be a Curie–Weiss paramagnet down to 2 K, similar to the formerly reported oxo-neptunyl (+2) **4** $NaNpO_2(CH_3COO)_3$. While, the N-substituted **2** and **3** are found to exhibit strikingly different magnetic features from the above oxo-neptunyls (+1, +2), such as strongly field (H)-dependent peculiar non-paramagnetic behavior up to 300 K for the both, and anomalous magnetic-relaxation (creep) behavior at low temperature for **2**, etc. Possible origin and implication of such anomalous magnetic features of **2** and **3** are argued based on the extensive magnetic data collected for over the past 1 year.

Keywords: Actinide alloys and compounds; Chemical synthesis; Precipitation; Crystal and ligand field; Hyperfine interaction; Magnetization; Magnetic measurement; Mössbauer spectroscopy; X-ray diffraction

1. Introduction

To elucidate the magnetic property of actinide (An; i.e., 5f) complexes is of particular interest from the viewpoint of actinide low-dimensional (low-D) molecular magnetism. For example, in neptunyl (+1, +2) (Np(V, VI): $5f^{2,1}$) complexes (more generally in actinyl complexes), strongly bonded linear (uniaxial) neptunyl (actinyl) $(O{=}Np(An){=}O)^{+1,+2}$ monocations (An = U, (Np), Pu, Am, etc.) with unpaired Np(An) 5f electrons exist as a single-molecule magnetic entity and form unique 0D, 1D to 3D network structure extended by the so-called 'cation–cation bond' (CCB) [1]. Though in the higher-divalent (+2) neptunyls (actinyls) the formation of such CCB network is generally less probable due to the enhanced mutual electrostatic repulsion, suitable chemical modification of neptunyl (actinyl) (+2) coordination environment, e.g., by substitution of non-nyl (equatorial) (and even nyl) oxygen(s) by other anion(s) such as nitrogen (and sulfur, etc.) (as is indeed done here), is expected to open a route to the synthesis of novel actinide molecular entities (mono-, poly-nuclear and supramolecular magnetic systems) with different bonding (and network) character. Recently, transition-metal (3d) and lanthanide (4f) clusters, rings and complexes have been attracting increasing interest as nanoscale and/or molecular magnets [2,3]. Since 5f electrons of the actinides are well known to exhibit a marginal character between the (more-itinerant) 3d and the

☆ The paper presented at Plutonium-Futures 2006 at Asilomar in 13 July.

* Corresponding author. Tel.: +81 29 284 3831; fax: +81 29 282 5939.
E-mail address: nakamura.akio@jaea.go.jp (A. Nakamura).

[1] Present address: Toray Research Center, Ohtsu, Shiga 520-8567, Japan.

0925-8388/$ – see front matter © 2006 Elsevier B.V. All rights reserved.
doi:10.1016/j.jallcom.2006.12.062

(more-localized atomic-like) 4f electrons [4], the extension of such study to actinides and further to their hybrid (i.e., 3d, 4f plus 5f) versions [5–7] will significantly enlarge our scope for nanoscale and/or molecular magnets.

The ^{237}Np-Mössbauer and magnetic study of several oxygen-coordinated (oxo) neptunyl (+1) (Np(V); $5f^2$) complexes of our group [8–12] has indeed revealed that, through unique interplay of strong uniaxial crystal electric field of the nyl-oxygens and the strong spin-orbit coupling of the 5f-electron systems, they exhibit intriguing common feature as an Ising-type neptunyl (+1)-molecular magnet and yet diverse character depending on the specific neptunyl (+1) CCB network structure from a Curie-para- to ferro- and meta-magnets. We have been recently extending such study to neptunyl (+2) (Np(VI); $5f^1$) complexes for which magnetic data are by far lacking, in addition to a trinitrato oxo-complex **1** $NH_4[NpO_2(NO_3)_2]$ [13], to two (acetylacetone(acac = $C_5H_7O_2^-$) or trinitrato) pyridine (py = C_5H_5N) complexes, **2** $NpO_2(acac)_2py$ [14] and **3** $NpO_2(NO_3)_2byp$ (bpy(bipyridine) = $C_{10}H_8N_2$). Here, as mentioned above, due to the higher (+2) neptunyl valence state (i.e., mainly due to their enhanced mutual electrostatic repulsion), such CCB network formation is generally less probable, and all these three (**1**–**3**) are in fact nominally 0D non-CCB systems. In this sense, the latter **2** and **3**, in which one and two of non-nyl oxygens are substituted with nitrogen (N), respectively, are regarded as our first-trial systems for chemically modifying such 'nyl'-based molecular structure and possibly realizing some alternative (non-CCB) network formation mechanism in the future.

The oxo-**1** was found to be a Curie–Weiss paramagnet over $T = 2$–300 K, similar to the formerly reported sodium neptunyl (+2) acetate **4** $NaNpO_2(CH_3COO)_3$ [15]. While, the N-substituted **2** and **3** were found to exhibit many striking magnetic features different from those of the above oxo-neptunyl (+1, +2) complexes: For example, the both showed peculiar field (H)-dependent non-paramagnetic behavior up to room temperature, which seems to imply the presence of minor ferromagnetic component (phase) with Curie temperature T_C well above 300 K ($T_C > 300$ K), and **2** showed anomalous magnetic relaxation (creep) behavior at low temperature. To be frank, there still remains some ambiguity whether such anomalous magnetic behavior of **2** and **3** is indeed due to such non-nyl oxygen → nitrogen substitution effect. One disturbing factor here is; only for these two systems (**2** and **3**), we were obliged to adopt different sample-sealing method for the SQUID magnetic measurements, the embedment in an organic resin (staycast), than that adopted for all other samples (simple sealing in a quartz ample). Including this problem of new sample-sealing method, possible origin and implication of these anomalous magnetic features of **2** and **3** are argued based on the extensive magnetic data collected for over the past 1 year.

Below, after the experimental section for the present three neptunyl (+2) complexes (**1**–**3**), we first describe and discuss the basic structural and electronic features of these neptunyl (+1, +2) complexes, essential for the understanding of their magnetic properties, based on their XRD and ^{237}Np-Mössbauer data. Thereupon, in subsequent sections, their unique (yet different) 'nyl'-based molecular-magnetic properties will be delineated and discussed, first for the neptunyl (+1) and then for the neptunyl (+2) complexes, the both of which being centered mainly on our own work. Thus, this paper is intended to be a (comprehensive) present-stage summary for this new area of actinide low-D molecular magnetism.

2. Experimental

2.1. Sample preparation

Polycrystalline powder samples of all the present neptunyl (+2) complexes (**1**–**3**) were prepared by wet-chemical methods reported by Alcock et al. for each system [16a–c]. As the preparation procedure of oxo-**1** is already given [13], only those of N-substituted **2** and **3** are briefly mentioned here. The starting $^{237}NpO_2$ powder was dissolved in concentrated HNO_3 solution by heating to a slight boil. The solution obtained was evaporated to wet salt. The dry residue was dissolved in distilled water, and the resultant Np(VI) solution was stocked in a glass flask. The neptunyl(VI) nitrate used as the starting material, $NpO_2(NO_3)_2{\cdot}xH_2O$, was obtained by evaporating this Np(VI) stock solution. All the synthesis and powder XRD analysis were made in a glove box at room temperature. To the 3 ml acetonitrile (CH_3CN) solution containing 250 mg of the neptunyl(VI) nitrate, either 0.15 ml of acetylacetone and 0.1 mol of pyridine (in case of **2**) or 150 mg of 2,2′-bipyridine (bpy) and 1 ml of acetonitrile (in case of **3**) were added. In either case, brown-colored powder precipitates are readily formed. Those were analyzed by powder XRD diffractometer (Rigaku RAD-3C) with Cu Kα radiation and were identified to be single phase materials of **2** and **3**, respectively.

2.2. ^{237}Np-Mössbauer measurements

The ^{237}Np-Mössbauer spectra were measured at 11–40 K in a cryostat equipped with a driving system (Wissel GmbH, MS II), using a sealed assembled ^{241}Am metal source (∼600 MBq) moving in sinusoidal driving mode [17a–c]. Velocity calibration was made by using a laser calibrator Wissel MVC 450. All the **1**–**3** samples used are their raw powders (containing no organic-resin solidifier) firmly encapsulated in a double inner-carbon and outer-Al container, the latter further being thoroughly indium-sealed. All the sample (absorber) thickness was ∼100 mg Np/cm^2. The Mössbauer data thus obtained were least-square fitted to Lorenzian lines using "IGOR" (Wave metrics, Lake Oswego, Oregon) software. As is well known and as is indeed the case for the present three systems, ^{237}Np-Mössbauer spectra of these neptunyls (+1, +2) occasionally exhibit the so-called paramagnetic-relaxation spectra. For the analysis of such spectra Wickman's relaxation model [18] was adopted.

2.3. SQUID magnetic measurements

DC magnetization (M) and magnetic susceptibility ($\chi = M/H$) of **2** and **3** were measured by a SQUID magnetometer (MPMS, QD) at 2–300 K at applied fields of $H = 0.002$–5.5 T using about 10 mg of respective powder samples embedded in a staycast (an organic epoxy resin). While, all the previous SQUID magnetic measurements of **1** [13] and the neptunyl (+1) complexes reported by our group [8–12] had been made simply by encapsulating their powders in quartz (or other) tube in inert (helium) atmosphere as in the case of above ^{237}Np-Mössbauer experiment (i.e., without using such organic resin). As mentioned formerly, the SQUID magnetic data of most-recently measured these two **2** and **3** employing this organic-resin sealant have exhibited many strikingly different peculiar features from those of other oxo-neptunyl (+1, +2) complexes. It is likely that such peculiar magnetic features of **2** and **3** are indeed originated from the non-nyl oxygen → nitrogen substitution in these systems. However, one interfering factor here is the effect of this new sample-sealing method. In fact, we have observed color change of sample **2** from brown to green during its 1–2 days embedment process into the organic resin (staycast), suggesting the occurrence of chemical reaction (most plausibly the Np(VI) → Np(V) reduction) around the sample surface-area. In order to identify possible origin including this chemical reaction with the organic-resin, the extent and the nature of such magnetic anomalies, we have made their extensive and repeated SQUID magnetic measurements over the

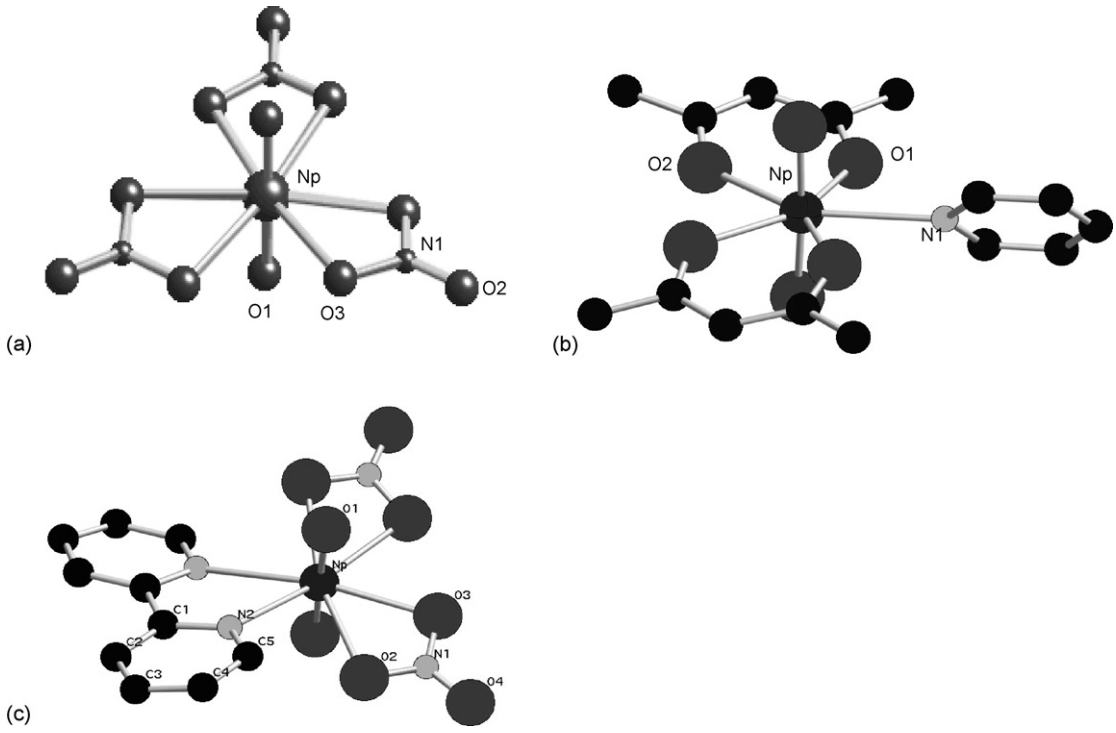

Fig. 1. Schematic depicting of coordination polyhedra around Np(VI) of the present three neptunyl (+2) complexes: (a) $NH_4[NpO_2(NO_3)_2]$ (**1**); (b) $NpO_2(acac)_2py$ (**2**); (c) $NpO_2(NO_3)_2byp$ (**3**).

past 1 year. For example, we have made detailed isothermal *M–H* curve measurements in small temperature interval ($\delta T = 10$–20°) throughout the 2–300 K range after about 10 months from their initial magnetic measurements (see Fig. 4b in brief).

3. Results and discussions

3.1. XRD and ^{237}Np-Mössbauer results of neptunyl (+1, +2) complexes

Fig. 1a–c shows the schematic coordination polyhedra around Np(VI) of the present three neptunyl (+2) complexes **1**–**3** based on the reported XRD data [13,16a–c]: the oxo-neptunyl (+2) **1** (Fig. 1a) has ideal hexagonal-bipyramidal structure (CN = 8) with two straight nyl-oxygens ($2O_{nyl}$s) ($\angle$O–Np–O = 180°) aligning parallel to the *c*-axis and six non-nyl (equatorial) oxygens ($6O_{eq}$s) from three bidentate trinitratos. One-nitrogen (1N) substituted **2** (Fig. 1b) has distorted pentagonal-bipyramidal structure (CN = 7) with significantly bent $2O_{nyl}$s ($\angle$O–Np–O = 176.5°) and largely buckling non-nyl $4O_{eq} + 1N_{eq}$ from two acetylacetone and a pyridine ligands, respectively. 2N-substituted **3** (Fig. 1c) has slightly distorted hexagonal-bipyramidal structure (CN = 8) with slightly bent $2O_{nyl}$s ($\angle$O–Np–O = 177.9°) and non-nyl $4O_{eq} + 2N_{eq}$ from two bidentate trinitratos and a biprydine, respectively. All these three have crystallographically only one kind of isolated Np(VI) site shown here (the nearest-neighbor (NN) Np(VI)–Np(VI) distance well over 4.5 Å in every case), and hence are classified nominally as 0D (non-CCB) mono-nuclear complexes.

For the sake of following discussion, we have listed in Table 1 relevant XRD and ^{237}Np-Mössbauer data of these three neptunyls (+2) **1**–**3** in Fig. 1 and of the formerly reported sodium acetate neptunyl (+2) **4** [15]. As is apparent, they all have extremely short (less than 1.80 Å) strongly covalent-bonded

Table 1
Structural and Mössbauer parameters of several neptunyl (+1, +2) complexes

Np(VI) or Np(V) compound	*D*[a]	CN[b]	Angle (°) (O_{nyl}–Np–O_{nyl})	Bond length Np–O_{nyl} (Å)	Bond length Np–O $(N)_{eq}$ (Å)	Quadrupole: e^2qQ (mm/s)	Magnetic: H_{eff} (T)
Np(VI): $NH_4[NpO_2(NO_3)_2]$ (**1**)	0	8	180	1.735	2.468	244	291
Np(VI): $NpO_2(acac)_2(py)$ (**2**)	0	7 (6O + N)	176.5	1.78	2.33–2.37 (2.56)	191	220
Np(VI): $NpO_2(NpO_3)_2(bpy)$ (**3**)	0	8 (6O + 2N)	177.9	1.728	2.47–2.49 (2.56)	239	296
Np(VI): $NaNpO_2(CH_3COO)_3$ (**4**)	0	8	180	1.766–1.787	2.456	238	270
Np(V): formates (**5**, **6**), phthalate (**7**), oxalate (**8**), mellitate (**9**), polymellitate (**10**)	0–2	7–8	175–180	1.82–1.85	2.37–2.60	88–100	500–550

[a] Dimensionality of the nyl-network.
[b] Coordination number.

basically linear unique neptunyl (+2) $(O_{nyl}{=}Np(VI){=}O_{nyl})^{+2}$ molecular structure, and additionally have weakly ionic-bonded several (generally four to six) non-nyl (equatorial) oxygens (O_{eq}s) at far-more distant position (∼2.3–2.5 Å). In both **2** and **3**, their respective one or two non-nyl nitrogens ($1N_{eq}$ or $2N_{eq}$s) in Fig. 1b and c substituting the O_{eq}s are known to locate at even more-distant position (∼2.56 Å) than the latter. The reported Shannon's ionic radii (CN = 4) are 1.46 Å for N^{3-} and 1.38 Å for O^{2-} [19]. So, this ionic-radii difference of 0.08 (=1.46 − 1.38) Å between N^{3-} and O^{2-} almost quantitatively accounts for the non-nyl bond-length difference between Np(VI)–$N_{eq}{}^{3-}$ and Np(VI)–$O_{eq}{}^{2-}$ in **3**, but, in **2** this is even more different than this ionic-radii difference, as seen in Table 1. Whereas, tetramethyl-ammonium neptunium (VI) isothiocyanate, $[N(CH_3)_4]_4[Np(NCS)_8]$, in which Np(VI) is eight-fold N coordinated (CN = 8) in a distorted tetragonal antiprism structure, is reported to have considerably shorter Np(VI)–N bonds ranging 2.39–2.42 Å [20]. These results imply that, contrary to our expectation that nitrogen (N) forms stronger covalent An–N bond than the ionic An–O bond, the N_{eq}s as well as their O_{eq}s in **2** and **3** are rather weakly ionic-bonded to the Np(VI). However, as will be seen below, such O → N substitution seems to have much greater direct as well as indirect structural and magnetic effects on the system than anticipated merely from this kind of bond-length (difference) consideration.

For comparison, we have also briefly listed in the last one line available data for several oxo-neptunyl (+1) complexes; two formates, **5** $NH_4[NpO_2(O_2CH)_2]$ and **6** $NpO_2(O_2CH)(H_2O)$, and a phthalate **7** $(NpO_2)_2(O_2C)_2C_6H_4(H_2O)_3$, reported by us, and an oxalate **8** $(NpO_2)_2(C_2O_4)(4H_2O)$ [21,22], mellitate and polymellitate, **9** $Na_4(NpO_2)_2(C_{12}O_{12})\cdot 8H_2O$ [23] and **10** $Na_3(NpO_2)(C_{10}O_8H_2)_2\cdot 11H_2O$ [24], reported by other groups in literature. The neptunyls (+1) are found to have slightly more-distant (less-uniaxial) O_{nyl}s (>1.80 Å) than the neptunyls (+2).

As for the ^{237}Np-Mössbauer data listed in the last two columns, the electric and magnetic splittings (e^2qQ and H_{eff}) of each system have been obtained through analysis of their well-known paramagnetic-relaxation spectra according to the Wickman's model (which assumes only an Ising-type spin up and down (flip-flop) configurations) (see [18] for the details). Fig. 2 shows one such typical relaxation spectrum at 11 K for **3** (those of **1** and **2** are reported in [13,25], respectively). As seen here, superimposed to the large electric-quadrupole splitting (e^2qQ) characteristic for these unique uniaxial neptunyl (+1, +2) molecules (largely distorted non-spherical electron distribution around the Np(V, VI)), though magnetically not long-range ordered (i.e., paramagnetic) in the measured T = 11–40 K range, the system gives either well-resolved magnetically split ^{237}Np-Mössbauer spectra due to the extremely slow relaxation rate; $\tau^{-1} < 10^9\ s^{-1}$ (τ: relaxation time) in this particular case (of course, in other faster relaxation case, more vague magnetically not so well-split spectra are often observed too) [13], and reveals clearly the presence of internal (hyperfine) magnetic field (H_{eff}) at the ^{237}Np(VI, V) nucleus through hyperfine interaction of their nuclear spin (I = 5/2 both in the ground and excited states) with very slowly fluctuating (flip-flopping) magnetic (spin plus orbital–angular) moments of the 5f electrons ($5f^{2,1}$) of the neptunyls (+1, +2) (Np(V, VI)). With increasing temperature, their relaxation time (τ/s) becomes shorter, i.e., the flip-flop rate (τ^{-1}) of the 5f magnetic moments becomes faster, and the Mössbauer spectra become increasingly broadened and obscured.

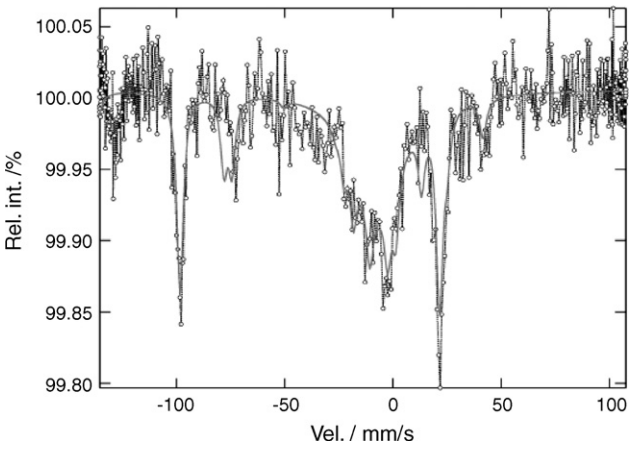

Fig. 2. ^{237}Np-Mössbauer spectrum of $NpO_2(NO_3)_2$byp (**3**) measured at 11 K. Solid line: simulated curve according to the Wickman's relaxation model [18].

One can immediately recognize in Table 1 that these individual near-linear neptunyl $(O{=}Np{=}O)^{+1,+2}$ monocations (molecules) have indeed very unique strongly axial-anisotropic crystal, electric and magnetic structures, yet their degree (strength) and nature of uniaxial anisotropy being varied to a significant extent with Np valence and chemical constitution (and construction) of the system. For example, among the four neptunyls (+2) listed here **1**–**4**, only the 1N-substituted **2** has distorted pentagonal-bipyramidal structure (CN = 7) and has definitely weaker structural axial anisotropy (the longer Np=O_{nyl} and shorter Np–O_{equ} bonds) compared with other three systems (two oxo-**1** and -**4** and 2N-substituted **3**) with near-ideal hexagonal-bipyramidal structure (CN = 8). That is, the bond-length ratio of Np=O_{nyl}/Np–O_{equ} (≪1) is definitely larger in **2** than those of the latter, hence, **2** has clearly much weaker (less axial-anisotropic) quadrupole and magnetic splittings (e^2qQ and H_{eff}) as shown there. Such weaker structural, electric and magnetic axial anisotropies of this 1N-substituted **2** (CN = 7) (Fig. 1b) is judged to result most plausibly from the overcrowding (steric hindrance) of bulky ligands (two acac(=$C_5H_7O_2^-$) plus a py(=C_5H_5N)) around the neptunyl (+2) in this system [16b]. This is directly reflected in its more (in fact most) distorted 'nyl' molecular structure ($\angle O_{nyl}$–Np–O_{nyl} = 176.5°) and non-planar bumpy non-nyl ($4O_{eq} + 1N_{eq}$) coordination, in contrast to the latter three systems (**1**, **3**, **4**).

It is also readily known in Table 1 that the neptunyls (+2) (Np(VI); $5f^1$) and (+1) (Np(V); $5f^2$) have significantly different electric and magnetic splittings. In short, the neptunyls (+2) have much larger e^2qQ than the neptunyls (+1), reflecting the stronger crystal-structural axial anisotropy in the former as seen there. But, the trend is just reversed for H_{eff}, reflecting here the more-magnetic nature of the ground-state electronic configuration in the neptunyl (+1) (Np(V); $5f^2$: J = 4 in $^3H_4$) than that in the neptunyl (+2) (Np(VI); $5f^1$: J = 5/2 in $^2F_{5/2}$) in the L–S coupling. These experimental e^2qQ and H_{eff} values are mostly in line with

Table 2
Brief summary of magnetic and related properties of several neptunyl (+1) ((NpV): $5f^1$) complexes

Np(V) compound	D	CN	T_C (K)	μ(eff)[a] (μ_B)	μ(sat)[a] (μ_B)	e^2qQ (mm/s)	H_{eff} (T)	Angle (°) (O_{nyl}–Np–O_{nyl})	Np–Np (Å)
Formate: $NH_4NpO_2(O_2CH)_2$ (**5**)	0	8	– (para)	3.32	1.6–1.72	108	550	180	4.04–4.14
Formate: $NpO_2(O_2CH)(H_2O)$ (**6**)	2	7	12.8 (ferro)	2.82	1.23	88.5	550	178.2	4.06–4.16
Oxalate: $[(NpO_2)_2(O_4C_2)]4H_2O$ (**8**)	2	7	11.6 (ferro)	2.71	1.2–1.3	92	550	178.1	4.075
Phthalate: $[(NpO_2)_2(O_2C)_2C_6H_4(H_2O)_3]$ (**7**)	2 (2Np sites)	7	4.5 (meta)	2.22–2.57	1.18–1.2	75	496	177.4 + 178.6	3.91–4.20
Mellitate: $Na_4(NpO_2)_2(C_{12}O_{12})\cdot 8H_2O$ (**9**) (poly mellitate: $(Na_3(NpO_2)(C_{10}O_8\ H_2))_2\cdot 11H_2O$) (**10**)	2′(dimer) (0)	7 (7)	10 (para)	4.61 (5.91)	–	97	549	172.7 (178.8)	3.482 (6.767)

[a] The free-ion ('nyl'-model) values for Np(V) ($5f^2$): μ(eff) = 3.58 (3.20)μ_B, μ(sat) = 3.20 (1.60)μ_B.

the reported theoretical calculations [26a and b], albeit in case of e^2qQ for neptunyl (+1) (and plutonyl (+2)) (i.e., $5f^2$) those in Table 1 are generally much smaller (∼1/2 or even less) than the calculated one.

3.2. Magnetic property of neptunyl (+1) (Np(V); $5f^2$) complexes

As mentioned formerly, the magnetic plus ^{237}Np-Mössbauer study of several oxo-neptunyl (+1) complexes of our group [8–12] has clarified their intriguing common feature as a 'nyl'-based molecular magnet and yet diverse character from a Curie–Weiss para- to ferro- and meta-magnets depending on the specific neptunyl (+1) CCB network structure. Before proceeding to the present three neptunyls (+2) case (**1**–**3**) (plus **4**) in Fig. 1 and Table 1, we first discuss here the magnetic properties of oxo-neptunyls (+1) for which more ample experimental data are available. For this purpose, augmenting the last line of Table 1, we have re-listed in Table 2 more in detail the relevant magnetic, ^{237}Np-Mössbauer and XRD data of these neptunyl (+1) complexes.

Among the listed total six neptunyls (+1) (**5**–**10**), in contrast to the neptunyls (+2) in Table 1, only the first formate **5** has 0D (non-CCB) near-ideal hexagonal-bipyramidal structure (CN = 8, ∠O_{nyl}–Np–O_{nyl} = 180°), and was found to be a Curie-paramagnet (or only marginal ferromagnetic) down to 2 K [9,10,12]. **5** has in fact a 1D chain structure along the c-axis direction. However, all the straight 'nyl' molecules are aligning here perpendicular to this 1D chain (∥ the b-axis), and in this sense **5** is 0D without CCB. The next three systems, i.e., one other formate **6** [8] and an oxalate **8** [21,22] and a phthalate **7** [11,12], the all are 2D CCB pentagonal-bipyramidal systems (CN = 7) with bumpy neptunyl (+1) 2D sheet (network). The former two (**6** and **8**) with single kind of Np site are ferromagnets with the highest Curie temperature of T_C ∼12–13 K reported for any neptunyl (+1, +2) complexes. On the other hand, the phthalate **7** is a metamagnet exhibiting a clear two-step magnetization (M–H) curve below its T_N ∼ 4.5 K, corresponding well to the 1:1 presence of the two kinds of Np sites [11,12].

Inspection of the listed data on these 0D to 2D oxo-neptunyls (+1) (**5**–**8**) in Table 2 indicates that the paramagnetic 0D **5** (CN = 8) has all the largest values of macroscopic magnetic (the effective-paramagnetic moment (μ(eff)) and the saturation moment (μ(sat))) as well as the microscopic ^{237}Np-Mössbauer (e^2qQ and H_{eff}) parameters. The latter three 2D CCB systems (**6**–**8**) (CN = 7), in spite of the observed magnetic ordering at low temperature, have generally smaller values of all these parameters, roughly in the order; 0D **5** (CN = 8) > 2D **6** and **8** (CN = 7) > 2D (+2Np sites) **7** (CN = 7). Since all these four systems have nearly the same NN Np–Np distance in the range 3.90–4.20 Å as shown there, the main origin for this clear trend is supposed to be concomitantly occurring (a) distortion of the linear 'nyl' (O=Np(V)=O) structure and (b) misalignment of the 'nyl' molecules in the latter 2D CCB systems (**6**–**8**) (CN = 7). That is, in the simplest 0D non-CCB **5** (CN = 8), as mentioned above, the near-ideal linear (180°) neptunyl (+1) molecules are all aligned just parallel to each other in the (only one) b-axis direction. In contrast, in 2D **6** and **8** (CN = 7), though they too have crystallographically only one kind of Np site, their neptunyl (+1) molecules are not only distorted (∠O=Np(V)=O < 180°) to form the bumpy 2D CCB sheet but also (mis)aligned at least along the two different directions within such bumpy 2D sheet [8–10]. Further in 2D-CCB **7** (CN = 7) with two kinds of Np sites they are more randomly (mis)aligned at least along four different directions in the even more-bumpy (more-buckling) 2D sheet [11,12].

Though not listed in Table 2 (for the non-availability of XRD- and ^{237}Np-Mössbauer data), Gruen and Huchison [15] reported the magnetic susceptibility (χ) data at T = 14–320 K for another neptunyl (+1) oxalate **11** $NpO_2(O_4C_2)(H_2O)_2$ (different from **8**). The reported data can be well expressed by the simple Curie law: χ (mol) = 1.257/T, giving μ(eff) = 3.17μ_B. This large value of μ(eff) close to that of **5** implies that **11** is most plausibly a 0D hexagonal-bipyramidal system (CN = 8) similar to **5**.

The above results demonstrate that the neptunyl (+1) CCB network formation (i.e., the neptunyl (+1)–neptunyl (+1) intermolecular interaction) is crucial for the onset of long-range magnetic order in these systems, and simultaneously illustrate the delicate influence of the individual 'nyl'-molecular structure and its way of alignment on their macroscopic as well as microscopic molecular-magnetic properties. It is also true that they all are basically simple Curie-type (localized $5f^2$-electrons)

paramagnets with no TIP term (χ_0(TIP) = 0) with their (powder-averaged) μ(eff) and μ(sat) both significantly quenched from the free-ion values for Np(V) ($5f^2$) in the L–S coupling ($^3H_4$: $J = 4$, $g_L = 4/5$): $\mu(\text{eff}) = g_L\mu_B[J(J+1)]^{1/2} = 3.58\mu_B$, $\mu(\text{sat}) = g_L J_Z \mu_B = 3.20\mu_B$. Together with the above-discussed well-known ^{237}Np-Mössbauer paramagnetic-relaxation spectra, one can reasonably guess that, through interplay of such strong uniaxial crystal electric field (CEF) of 'nyl' oxygens and the strong spin-orbit coupling (characteristic only for these 5f-electron systems), these individual neptunyl (+1) monocations (Np(V): $5f^2$) are indeed behaving here as an unique Ising-type single-molecule magnetic entity with its principal magnetization axis ($\parallel J_Z = \pm 4$: the ground state non-Kramers doublet) tightly confined along the linear neptunyl-bond direction. We have formerly proposed a theoretical treatment along this line and have succeeded to some extent in interpreting the above basic magnetic features of these neptunyl (+1) systems [9,10,12]. The derived powder-averaged theoretical χ^{-1} versus T and M versus H curves for the simplest 0D **5** have been shown to give a better agreement to their experimental curves than the free-ion curves. In short, the derived powder-averaged values of $\mu(\text{eff}) = 3.20\mu_B$ and $\mu(\text{sat}) = 1.60\mu_B$ [9,10] for our 'nyl' model are in fair agreement with the respective experimental values for **5** listed in Table 2.

Some remarks are appropriate here for the last two systems listed in Table 2, mellitate and polymellitate complexes, **9** and **10** [23,24]. From the XRD structural analysis, the mellitate **9** is reported to be the first example of neptunyl (+1) dimer composed of mutually coordinating largely distorted (172.7°) two 'nyl' molecules with exceptionally short NN Np–Np distance (~3.482 Å). In addition, this system is reported to exhibit magnetic order at ~10 K. However, no detailed magnetic data (e.g., whether ferro or antiferro, and its μ_{sat} value, etc.) are not reported up to now. The only reported magnetic data are χ^{-1}–T plots at T = 10–250 K for the both [24]. The obtained very large value of μ_{eff} (=4.61μ_B) for this dimer **9** and its still larger value (=5.91μ_B) for the 0D polymellitate **10**, the both far exceed even the free-ion value (3.58μ_B) in the L–S coupling, and seem difficult to reconcile with the above majority of magnetic data for the oxo-neptunyls (+1). Reinvestigation of detailed magnetic properties of these two systems seems necessary and worthy.

We also note here that recently Albrecht-Schmitt et al. [27a–d] have been extending such XRD-structure and magnetic study to more-complex double (and triple)-salts type neptunyl (+1) (and actinyl) compounds containing other (non-magnetic) metallic centers (Ag, Se, etc.). A novel 3D CCB mixed-valent Np(IV)/Np(V) selenite with three kinds of Np sites, $Np(NpO_2)_2(SeO_3)_3$, is reported to be a Curie paramagnet down to 5 K with μ(eff) = 2.28μ_B [27b]. A 3D CCB β-$AgNpO_2(SeO_3)$ with two kinds of Np(V) sites (both CN = 7) has lately been found to be a ferromagnet with $T_C \sim 8$ K [27c]. Most importantly, with grown single crystals, in addition to the single-crystal XRD structure determination, they have measured its anisotropic magnetic property along different crystallographic directions. Though this attempt does not seem to have been fully successful interfered with sample to sample variation of minor Np(IV) content, etc., the reported values of μ(eff) (=2.32–3.19μ_B) and μ(sat) (=0.80–1.2μ_B) are qualitatively consistent with the above majority of the magnetic data for oxo-neptunyl (+1) complexes. These attempts altogether appear to be a promising next step toward exploration of novel anisotropic (low-D) actinide magnetic systems and further of their 3d, 4f hybrid versions.

3.3. Magnetic property of neptunyl (+2) (Np(VI); $5f^1$) complexes

We finally describe and discuss the results of most-recent magnetic study of our group on the three neptunyl (+2) complexes (**1**–**3**) with Np(VI) ($5f^1$) in Fig. 1 and in Table 1: the ground state electronic configuration for the free ion; $^2F_{5/2}$ in L–S coupling. Compared with the above-discussed neptunyls (+1) complexes, magnetic data of neptunyls (+2) are by far sparse, and almost the only one system for which we could find both the magnetic and ^{237}Np-Mössbauer data was this sodium acetate neptunyl (+2) complex **4** $NaNpO_2(CH_3COO)_3$ [15,26a] listed in Table 1. This seems to reflect the well-known fact that, among the multiple valence states of Np from Np(III) to Np(VII), Np(V) is the most stable in air and at room temperature, and even the third (next to Np(IV)) stable Np(VI)-containing compounds including the present neptunyls (+2) tend to be reduced (and decomposed) to the Np(V)-containing ones in prolonged (or in some case even in short) time scale. With this precaution in mind, we have attempted a first systematic study on the molecular-magnetic properties of these neptunyl (+2) complexes.

3.3.1. Oxo-neptunyls (+2): $NH_4[NpO_2(NO_3)_2]$ (**1**) and $NaNpO_2(CH_3COO)_3$ (**4**)

As shown in Table 1 and discussed above, the two 0D oxo-neptunyl (+2) complexes **1** and **4** have quite similar near-ideal hexagonal-bipyramidal structure (CN = 8) ($\angle O_{nyl}$–Np(VI)–O_{nyl} = 180°) (Fig. 1a), all the linear neptunyl (+1) molecules aligning in each only one crystallographic direction ($\parallel$ the c-axis and b-axis, respectively). In this sense, they are neptunyl (+2) analogues of the 0D neptunyl (+1) formate **5** (CN = 8) in Table 2. The both (**1** and **4**) have therefore very-alike high(est) values of quadrupole and magnetic splittings. Yet, in detail, the reported slightly smaller values of both these parameters (e^2qQ = 238 mm/s and H_{eff} = 270 T) in **4** than those in **1** (e^2qQ = 244 mm/s and H_{eff} = 291 T) seem to reflect consistently the slightly smaller structural 'nyl' axial anisotropy (the longer Np–O_{nyl} and shorter Np–O_{eq}) in **4** than in **1** in Table 1.

The χ^{-1}–T data of the both systems are shown in Fig. 3 and again give very-similar slightly convex (Curie–Weiss type paramagnetic) curves, reinforcing their structural and Mössbauer similarities. Down to 2 K, no sign of magnetic order has been detected, as in the case of the 0D neptunyl (+1) formate **5**. The least square fitting of the measured data of **1** to the Curie–Weiss law of the type, $\chi = \chi_0 + C/T$, where C is the Curie constant (=0.125μ(eff)^2), results in the following expression (the solid line in Fig. 3); $\chi = 4.23 \times 10^{-4} + 0.390/T$. While, that for **4** originally reported in [15] (the dotted curve) is: $\chi = 2.40 \times 10^{-4} + 0.425/T$. Thus, we obtain as the respective magnetic parameters, μ(eff) = 1.766μ_B and $\chi_0 = 4.23 \times 10^{-4}$ emu/mol for **1**, and

Table 3
Brief summary on the magnetic properties of neptunyl (+2) complexes

0D Np(VI) compound	CN	Curie–Weiss equation[a] $\chi = \chi_0 + C/T$ (emu/mol)	μ(eff)[a] (μ_B)	χ_0(TIP)[a] (emu/mol)	μ(2 K, 5.5 T) (μ_B)	M_{ferro}[a] (emu/mol)
$NH_4[NpO_2(NO_3)_2]$ (**1**)	8	$4.23 \times 10^{-4} + 0.390/T$	1.77	4.23×10^{-4}	0.81	–
$NpO_2(acac)_2(py)$ (**2**)	7 (6O + N)	$2.01 \times 10^{-3} + 1.378/T$	3.32	2.01×10^{-3}	1.42	46.8 ± 0.4
		$2.12 \times 10^{-3} + 1.398/T$	3.34	2.12×10^{-3}	1.50	52.5 ± 0.5
$NpO_2(NpO_3)_2(bpy)$ (**3**)	8 (6O + 2N)	$1.72 \times 10^{-3} + 0.287/T$	1.52	1.72×10^{-3}	0.32	10.0 ± 0.3
		$1.70 \times 10^{-3} + 0.380/T$	1.75	1.70×10^{-3}	0.35	14.6 ± 4.4
$NaNpO_2(CH_3COO)_3$ (**4**)	8	$2.4 \times 10^{-4} + 0.425/T$	1.84	2.40×10^{-4}	–	–

The free-ion ('nyl'-model) values for Np(VI) ($5f^2$): μ(eff) = 2.53 (2.14)μ_B, μ(sat) = 2.14 (1.07)μ_B.
[a] For **2** and **3**, the upper = initially measured data, and the lower: after ~10 months from the initial measurements.

μ(eff) = 1.844μ_B and $\chi_0 = 2.40 \times 10^{-4}$ emu/mol for **4**. These are listed in Table 3. The inset of Fig. 3 shows the *M*–*H* data of **1** at low temperature region. From this, μ(sat) is obtained. However, since no saturation is actually attained in the *M*–*H* curve even at *T* = 2 K and *H* = 5.5 T for all the present three systems **1**–**3**, this quantity is denoted in Table 3 as μ(2 K, 5.5 T). This parameter is not reported for **4**.

As a note added in proof, for **1** we have in fact briefly reported in [13] the χ^{-1}–*T* data measured at *H* = 0.1 T giving significantly steeper and oppositely concave curve (see Fig. 6 of [13]). In Fig. 3 those are replaced with the more-reliable higher-field (*H* = 0.5 T) data. The reason for this replacement is that the previous *H* = 0.1 T data give seemingly irrelevant much-more strongly *T*-dependent parameters; μ(eff) = 1.70μ_B and $\chi_0 = -2.76 \times 10^{-4}$ emu/mol at higher-*T* (>150 K) range and μ(eff) = 1.77μ_B and $\chi_0 = -4.75 \times 10^{-4}$ emu/mol at lower-*T* (<150 K) range. That is, the *H* = 0.1 T data at 2–300 K can neither be well expressed by a single Curie–Weiss curve, nor the resultant negative values of χ_0(TIP) (<0) in either temperature range seem reasonable, suggesting some experimental (or some other) problem involved here. One such plausible problem is the slow initial *M* rise of the low temperature *M*–*H* curves at low field region (*H* < ~0.2 T) seen in the inset of Fig. 3. This naturally results in the smaller χ(=*M*/*H*) (i.e., the larger χ^{-1})

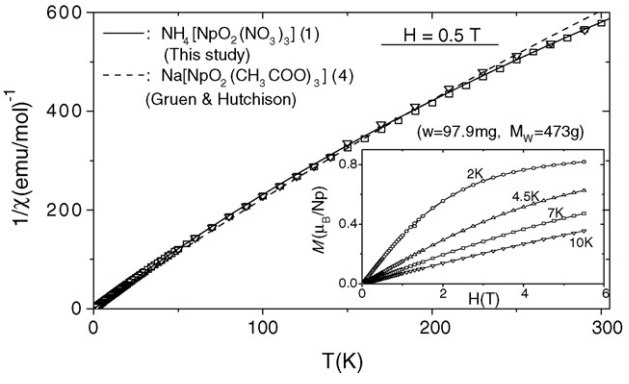

Fig. 3. Reciprocal magnetic susceptibility (χ^{-1}) vs. *T* plots of $NH_4[NpO_2(NO_3)_2]$ (**1**). (▽, □) Experimental data obtained in the ZFC and FC modes, respectively (sample weight: *w* = 97.9 mg; molecular weight: M_W = 473 g). Solid line: the calculated curve. Dotted line: $NaNpO_2(CH_3COO)_3$ (**4**) [15]. Inset shows the *M* (μ_B/Np) vs. *H*(*T*) plots of **1** at low temperature region.

value at *H* = 0.1 T than that at *H* = 0.5 T, as is indeed observed above between the two χ^{-1}–*T* curves up to *T* = 300 K measured at *H* = 0.1 and 0.5 T in the usual T-scan mode. However, unfortunately, we had not measured higher-temperature (>10 K) *M*–*H* curves of **1**. And this lack of higher-temperature (*T* = 20–300 K) *M*–*H* data prevents us to make an independent check of such steeper and oppositely concave *M*–*T* curve obtained for *H* = 0.1 T over the wide temperature range up to 300 K. Accordingly, accepting the general view that the lower field (=0.1 T) data are more susceptible to magnetic interference by minor magnetic impurities, the more-reasonable higher-field (=0.5 T) data are adopted in Fig. 3. As will be discussed below and readily seen in Figs. 4 and 5, we have encountered the similar situation (but having just the reverse tendency that higher the *H* lower the χ) in the magnetic data of **2** and **3**, and there this lesson from the present case study for **1** has been fully utilized.

Since the above Curie–Weiss expression for **4** was derived by curve-fitting to much smaller number of data points (total 11 at *T* = 14, 20, 62, 77, 131, 185, 195, 240, 274, 298 and 320 K) exhibiting either much-larger experimental scatter, the both sets of data for **1** and **4** shown in Fig. 3 would be eventually regarded as almost indistinguishable single set of data obtained for the same system (sample). Thus, one can mention here that the 0D oxo-neptunyl (2+) complexes with near-ideal hexagonal-bipyramidal structure (CN = 8) are Curie–Weiss-type (localized $5f^1$ (Np(VI)) electron) paramagnet having their magnetic parameters (μ(eff), χ_0(TIP) and μ(sat)) at most in the range covered by those obtained for these two complexes **1** and **4** of this type listed in Table 3: μ(eff) = 1.766–1.844μ_B, χ_0(TIP) = (4.23–2.40) × 10^{-4} emu/mol and μ(sat) = 0.8–0.85 μ_B.

The presence of χ_0(TIP) term which accounts for the small convex curvature of the χ^{-1}–*T* plots in Fig. 3 is characteristic for the oxo-neptunyls (+2) different from the above-oxo-neptunyls (+1) for which almost always χ_0(TIP) = 0 is found. According to our proposed theoretical model [9,10], this implies that in these oxo-neptunyls (+2) (Np(VI); $5f^1$) not only the ground Kramers doublet ($J_Z = \pm 5/2$) but also the relatively low-lying excited state ($J_Z = \pm 3/2$ or else) split by the axial neptunyl (+2) crystal electric field will contribute to the magnetic susceptibility (χ) of the system. Leaving such detailed analysis for future study, we only compare here the experimental magnetic parameters with their free-ion values for Np(VI) ($5f^1$:

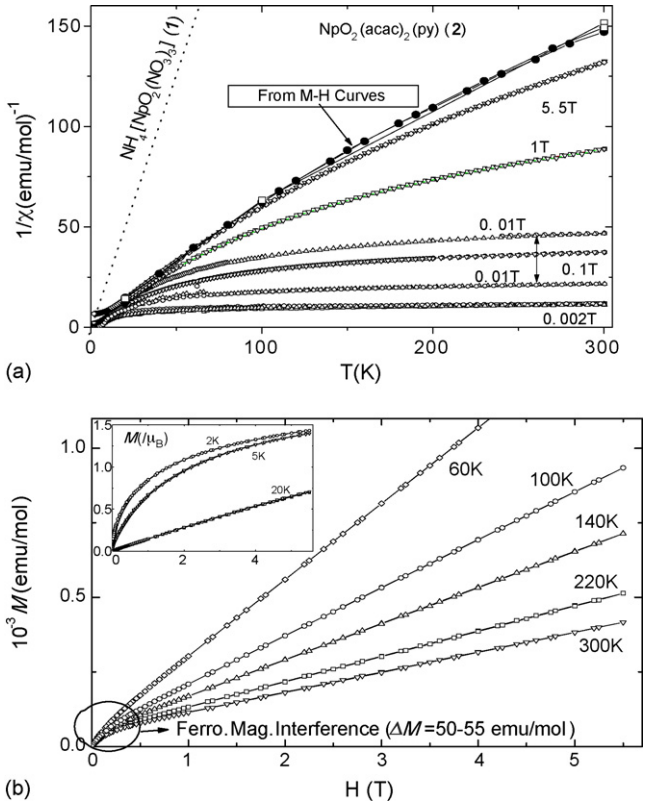

Fig. 4. (a) χ^{-1} vs. T plots of $NpO_2(acac)_2py$ (**2**) ($w = 14$ mg, $M_W = 546.4$ g). Smaller open symbols: data obtained from the M–T (K) measurements at various constant magnetic fields (Hs). Larger symbols (□, ●): data from the M–H curve measurements at various temperatures (initial and after 10 months, respectively) (see text for the details). Dotted line: χ^{-1}–T plot of **1** shown in Fig. 3. (b) Several representative M vs. H curves for $NpO_2(acac)_2py$ (**2**) at higher temperature region above 20 K after 10 months ($w = 14$ mg, $M_W = 546.4$ g). Bulk χ of the system at each T (K) was determined from the higher field ($H > \sim 0.5$ T) linear M–H portion as $\chi = M/H$, and from its extrapolation to the zero filed ($H = 0$ T) small ferromagnetic component at each temperature was evaluated (see text for details). Inset also shows the initial M–H curves at low temperature region below 20 K for the same system.

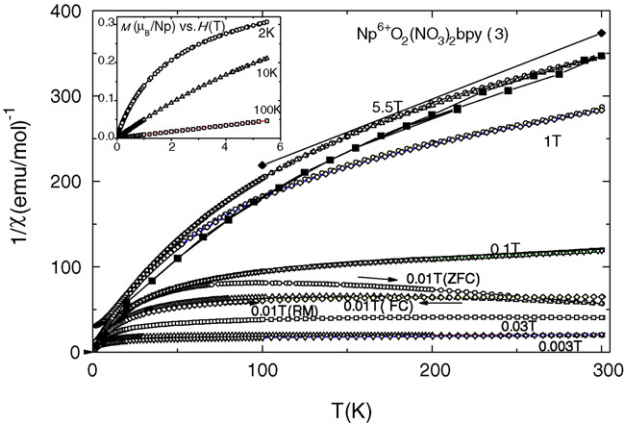

Fig. 5. χ^{-1} vs. T plots of $NpO_2(NO_3)_2byp$ (**3**) ($w = 12$ mg, $M_W = 549.2$ g). Smaller open symbols: data from the M–T measurements at various constant magnetic fields (Hs). Larger filled symbols (♦, ■): data from the M vs. H measurements at various T (K)s (initial, after 10 months) (see text for details). Inset shows the initial M–H curves at 2, 10 and 100 K.

$^2F_{5/2}$; $J = 5/2$, $g_L = 6/7$); $\mu(\text{eff}) = 2.53\mu_B$ and $\mu(\text{sat}) = 2.14\mu_B$, and with those for our proposed 'nyl' model including only the ground-doublet ($J_Z = \pm 5/2$) contribution; $\mu(\text{eff}) = 2.14\mu_B$ and $\mu(\text{sat}) = 1.07\mu_B$. Here again, as in the above neptunyl (+1) case (**5** in Table 2), the (powder-averaged) experimental values of both $\mu(\text{eff}) = 1.766$–$1.844\mu_B$ and $\mu(\text{sat}) = 0.8$–$0.85\mu_B$ for **1** and **4** are significantly quenched from the free-ion values, and show better agreement with our 'nyl' model.

*3.3.2. Nitrogen (N)-substituted $NpO_2(acac)_2py$ (**2**) and $NpO_2(NO_3)_2byp$ (**3**)*

Figs. 4a and 5 show the χ^{-1}–T data of the 1N-substituted $NpO_2(acac)_2py$ (CN = 7) **2** and the 2N-substituted $NpO_2(NO_3)_2byp$ (CN = 8) **3**, respectively. For comparison, χ^{-1}–T curve of **1** is also shown in Fig. 4a. At a glance, one can easily realize that both these two N-substituted systems **2** and **3** exhibit strikingly different magnetic behavior from those of the oxo-(+2) **1** and **4** (Fig. 3) discussed above. Both of these data measured in the usual T-scan mode at various magnetic fields ($H = 0.002$–5.5 T) show strongly H-dependent peculiar non-paramagnetic behavior, apparently shifting from a T-independent Van-Vleck type to a Curie–Weiss type with increasing H. In addition, as seen here for the two set of χ^{-1}–T data measured at the same $H = 0.01$ T for **2**, the low-field data of the both systems often exhibit significant run to run variation, even violating there-observed regular trend that higher the H larger the χ^{-1} (i.e., smaller the χ). And in **3**, as seen in Fig. 5 for $H = 0.01$ T data measured with the different ZFC (zero-field cooled), FC (field-cooled) and RM (remnant-magnetization) modes, the low-field χ^{-1} data sometimes have even a broad hump over extended intermediate temperature range (~50–200 K) below 300 K.

Also as for the magnitudes of χ, among the four neptunyl (+2) complexes (**1**–**4**) in Table 1, the 1N-substituted **2**, the only one system with largely distorted pentagonal-bipyramidal structure (CN = 7) (Fig. 1b), has by far the largest χ values (the smallest χ^{-1} values) and then mostly comes the 2N-substituted **3** (CN = 8): i.e., they are in the order; **2** (CN = 7) ≫ **3** (CN = 8) > **1** and **4** (CN = 8) for majority of their χ data. However, at low-temperature range ($T < \sim 20$ K), the latter inequality between **3** and **1** (and **4**) is reversed for higher-field ($H > \sim 1$ T) region. This can be more easily realized by comparing the respective M–H data at low temperature region shown as the insets of Figs. 3, 4b and 5 for **1**, **2** and **3**, respectively; at the lowest $T = 2$ K and the highest $H = 5.5$ T, **2** has surely the largest μ(2 K, 5.5 T) value (~$1.5\mu_B$), but **3** has the smallest value (~$0.3\mu_B$), and in between comes **1** (~$0.8\mu_B$). That is, **2** (CN = 7) > **1** and **4** (CN = 8) > **3** (CN = 8) for the μ(2 K, 5.5 T), as listed in Table 3.

A simple summary of the above-detailed peculiar χ^{-1}–T behavior of **2** and **3** is that with decreasing field (H) the both tend to have increasingly larger and less-temperature-dependent (finally nearly constant) χ (=M/H) over the wide temperature range up to 300 K. This is just reverse to the above situation in **1** that the lower $H = 0.1$ T gives the smaller χ than the higher $H = 0.5$ T. From these results, we have become aware of a possibility that in both **2** and **3** some minor ferromagnetic com-

ponent (or impurity) with Curie temperature T_C well over 300 K ($T_C > 300$ K) is giving rise to strong magnetic interference with their measured χ^{-1}–T curves especially at lower-field region. To verify this possibility, making use of the above lesson from the data-selection problem ($H = 0.1$ or 0.5 T data) in **1**, we have made detailed M–H curve measurements at small $\delta T = 10$–20° interval over the whole 2–300 K range for the both systems. These measurements were in fact most thoroughly performed nearly after 10 months from their initial SQUID magnetic measurements in which most of the χ^{-1}–T data (in Figs. 4a and 5 for **2** and **3**, respectively) and much fragmental low-temperature M–H data (in insets of Figs. 4b and 5 for **2** and **3**, respectively) have been measured.

Fig. 4b (the main figure) shows several selected higher-temperature (>50 K) M–H curves of **2** obtained in these recent detailed measurements. Obviously, these isothermal M–H curves of **2** at $T = 20$–300 K range all exhibit steep initial M rise responsible for such peculiar strongly H-dependent χ^{-1}–T curves in Fig. 4a, followed by more gradual linear M change with H at higher-field region for $H > \sim 0.5$–1 T. From the latter linear higher-field M–H portion, the χ (=M/H) at each temperature can be evaluated, and all the thus-obtained (now H-nondependent) χ values at various temperatures between 20 and 300 K are plotted in Fig. 4a as large filled symbols. While, the small ferromagnetic (FM) interference ΔM(ferro) that quickly saturates at low-field region ($H < 0.5$–1 T) at each temperature was evaluated by extrapolating the higher-H linear M–H curve to $H = 0$ T. This gives almost the constant value of ΔM(ferro) = ~50–55 emu/mol for all $T = 20$–300 K. Provided that this is due to, e.g., a FM iron (Fe) impurity ($\mu_{sat} \sim 2\mu_B$), the obtained ΔM(ferro) is estimated to be a Fe content of ~0.45–49 mol% level. Though data points are far more sparse ($T = 20$, 100 and 300 K), such H-nondependent χ can be also evaluated for the initial fragmental M–H curve data (only that at $T = 20$ K is shown in the inset of Fig. 4b), and these initial χ values are also plotted in Fig. 4a as large open symbols.

3 was also found to have analogous M–H curves to **2** in Fig. 4b but with much smaller FM interference, ΔM(ferro) = ~10–15 emu/mol (corresponding to ~0.09–0.13 mol% level FM-impurity content), though the raw M–H data are not shown here. The obtained χ^{-1}–T data are shown in Fig. 5 for both the initial fragmental ($T = 100$ and 300 K) and recent detailed measurements. These respective two sets of χ^{-1}–T data obtained from the M–H curve measurements shown in these Figs. 4a and 5 tell us that (1) even the highest field $H = 5.5$ T data measured in the usual T-scan mode are not naturally free from such FM interference and (2) the χ of **3** has changed (increased) much-more rapidly than that of **2** in this period (~10 months), though its value itself is much smaller than the latter.

The obtained (H-nondependent) χ^{-1}–T plots of (presumably bulk) **2** and **3** (in the sense that the both are free from each FM interference ΔM(ferro)) shown in Figs. 4a and 5, respectively, can be well represented by the Curie–Weiss law: $\chi = \chi_0 + C/T$, and their actual Curie–Weiss expressions, the derived values of μ(eff) and χ_0(TIP) are summarized in Table 3 for both the initial and recent M–H curve measurements for the either system, together with their other magnetic parameters; μ(2 K, 5.5 T) and ΔM(ferro). Though, as mentioned above, data points from the initial (fragmental) M–H curve measurements are certainly very small ($T = (20)$, 100 and 300 K), we can obtain sufficiently accurate numerical values of all these listed magnetic parameters either in these cases. This is because we can perform their data analysis in full reference to the derived high-accuracy Curie–Weiss expressions obtained for the recent detailed measurements for the either system.

Close inspection of the listed magnetic parameters (μ(eff), χ_0(TIP), μ(2 K, 5.5 T) and ΔM(ferro)) of **2** and **3** in Table 3 reveals that during these 10 months passed between the initial and recent M–H curve measurements almost all of these parameters for the both systems, except for the χ_0(TIP) of **3**, have definitely become larger (increased) to each different degree. This means that some kind of chemical and therefore magnetic modifications of the system is steadily proceeding with time in both **2** and **3**, adding up to their 'initial' high-T_C (>300 K) FM component (phase) (ΔM(ferro)). Though more experimental data are certainly necessary, we tentatively propose here two most-probable origins and/or mechanisms for such chemical modifications of the system:

(1) Chemical attack to these **2** and **3** powder samples by the staycast (an organic epoxy resin) used for the first time to seal them for the present SQUID measurements. As mentioned formerly, this sealing method was first applied to respond to the recently tightened safety requirement for RI handling. Since such chemical attack is considered to occur most severely within initial 1–2 days during the ring-opening solidification process of the staycast around the powder surface area in direct contact with it, this origin (mechanism) is judged to be responsible mainly for the initial-stage generation of near-surface FM components (the initial ΔM(ferro) listed in Table 3) for the both systems. Note here that during this initial (1–2 days) solidification process the color of **2** has in fact changed completely from brown to green, most plausibly suggesting that Np(VI) of this 1N-substituted neptunyl (+2) **2** at near-surface powder area has been reduced to Np(V) to a significant extent. While, such was not at all observed for **3**, maintaining its original brown color up to now. This difference in the initial color change of **2** and **3** seems to accord with the observed large and much smaller ΔM(ferro)s in the respective systems, i.e., $46.8 \rightarrow 52.5$ for $\mathbf{2} \gg 10 \rightarrow 15$ emu/mol for **3** in Table 3, showing also the respective subsequent changes over these 10 months by the arrows ($\rightarrow$). This means that **2** powder had been much more severely chemically attacked by the ring-opening solidification reaction of the staycast and hence indeed generated much larger initial amount of near-surface high-T_C (>300 K) FM component (phase) than **3**. Though how deep into the powder interior this chemical attack has penetrated is not clear, this is inferred to be very limited only to its near-surface area, judging from the fact that these ΔM(ferro)s only correspond to a quite small total amount of FM phase (well less than 1%) for the both systems, as estimated above.

(2) Self-radiation damage by α-decay of ^{237}Np nucleus: This origin (mechanism) is due to the intrinsic nuclear property of the main constituent, the radioactive ^{237}Np, distributed homogeneously inside the whole powder sample. So, contrary to the above (1), this is judged to be operating continuously everywhere in the powder **2** and **3** samples throughout, and hence to be responsible mainly for the subsequent steady chemical and magnetic changes of the system, i.e., the long-term steady increase of these magnetic parameters in these 10 months in Table 3. As mentioned above, rather in reverse, the long-term increase of ΔM(ferro) during these 10 months is much more pronounced in **3** (∼1.5 times) than in **2** (only ∼1.12 times), and this clearly indicates that some origin (mechanism) other than the chemical attack by the staycast would exist here, for, if the latter alone is operating, **2** should exhibit the larger long-term ΔM(ferro) increase than **3** either here. As such chemical attack is considered to finish mostly in 1–2 days within the initial ring-opening solidification of the staycast, the observed relatively large long-term ΔM(ferro) change over these 10 months (∼5–6 emu/mol for the both systems) seems to be too large to be attributed only to this origin. Moreover, as discussed above, the derived magnetic parameters (μ(eff), χ_0(TIP) and μ(2 K, 5.5 T)) of both **2** and **3** powder-interior bulk phases, free from such near-surface high-T_C (>300 K) FM component (phase), also exhibit similar long-term increase (also larger in **3** than in **2**), reinforces our supposition that one other different mechanism, here-proposed (2), is also operating as one such causing magnetic (and chemical) alteration of the whole system including both the bulk-interior and near-surface (already initially chemically modified) areas of either **2** or **3** powder sample. Though we are not aware of any literature report on this kind of long-term self-radiation damage effect on the neptunyl (+1, +2) complexes, this seems likely in view of rather fragile nature of these materials.

Whereas, the (worst) possibility that such high-T_C (>300 K) FM component (maximum well below ∼1 mol% level) would be a (fixed amount of) extrinsic FM metal (or its oxide) impurity such as iron (Fe) (or Fe_3O_4, etc.) seems to be excluded because of the above very fact that the ΔM(ferro)s are changing (increasing) with time. We will return to this problem shortly later, and in the below first discuss the derived bulk magnetic properties of **2** and **3** supposed to be free from such FM interference.

Several characteristic magnetic features of these N-substituted **2** and **3** are apparent in Table 3. First, **2** is found to have all the largest values of these magnetic parameters (μ(eff), χ_0(TIP) and μ(2 K, 5.5 T)) with all their relatively small changes over these 10 months. Particularly, very high value of μ(eff) = 3.32–3.34μ_B exceeds significantly the free-ion (and our proposed 'nyl'-model) values of 2.53 (2.14)μ_B for Np(VI), approaching to those for Np(V), 3.58 (3.20)μ_B in Table 2. Also its μ(2 K, 5.5 T) exceeds the 'nyl'-model value of 1.07μ_B, but is still smaller than the free-ion value of 2.14μ_B. It is tempting to relate this exceptionally large value of μ(eff) = 3.32–3.34μ_B of the largely distorted neptunyl (+2) **2** (CN = 7) to that (μ(eff) ∼ 4.6μ_B) of the more-severely distorted neptunyl (+1) dimmer **9** in Table 2. In addition, **2** has χ_0(TIP) (2.01–2.12 × 10^{-3}) almost five times to one order of magnitude as large as those of the oxo-**1** and -**4**. It is inferred that such some kind of exceptionality of macroscopic magnetic features of **2**, as well as that of its microscopic Mössbauer features in Table 1, are associated with its largely distorted pentagonal-bipyramidal structure (CN = 7) brought about by the non-nyl O → N substitution. As mentioned formerly, only **2** has much weaker uniaxial 'nyl'-molecular, electric and magnetic structures in Table 1.

On the other hand, the 2N-substituted **3** has more ideal (less-distorted) hexagonal-bipyramidal structure (CN = 8) similar to the oxo-**1** and -**4**, and its microscopic Mössbauer (electric and magnetic) features are equally very alike to the latter (Table 1). Indeed this system has similar magnetic parameters to the latter (μ(eff) = 1.52–1.75μ_B and μ(2 K, 5.5 T) = 0.32–35μ_B), except for its large χ_0(TIP) similar to **2**. It is also found in Table 3 that, though the initial ΔM(ferro) of **3** itself is relatively small (about one-fourth (1/4) of that of **2**), this as well as its bulk magnetic parameters (μ(eff), μ(2 K, 5.5 T)) have changed more-significantly than those of **2** during these 10 months.

Apparently, our weak-point in the above discussion is that at present we cannot ascribe such anomalous magnetic behavior of **2** and **3** definitely to the non-nyl O → N substitution effect (and its caused structural modification effect) of the system, due to the presence of additional interference effects from the above-mentioned new sample-sealing method (and the above two origin and mechanism (1) and (2)). To prove or disprove the above argument on the chemical modifications of neptunyl complexes, additional experiments are certainly necessary. The most-direct experiment is to replace the present exopy-resin (staycast) sealant to chemically inert one such as paraffin, etc., that does not chemically attack the powder sample, or, as previously done, to encapsulate (seal) the raw powder sample directly in quartz (or other) tube without using any organic-chemical sealant. Though the conventionally used last method seems difficult to apply (as it is) due to the current RI-safety requirement, to perform long-term careful and detailed SQUID magnetic measurements of **2** and **3** (and also of other oxo-**1**, etc.) again employing either of the latter powder-sealing methods is of vital importance for deciding whether or not the here-observed minor high-T_C (>300 K) FM component (phase) is really a chemically modified surface phase of **2** and **3** generated through involvement in the ring-opening solidification process of the staycast. This is because up to now such high-T_C (>300 K) FM Np-containing compound, whether neptunyl-complex type or any other non-metallic inorganic compound, has never been reported. More cautiously, such experiments are necessary to conclude whether the present minor high-T_C (>300 K) FM phase is indeed not a FM metallic origin (e.g., Fe or Co, their some oxides, or oxo-complexes, etc.), and in addition, to confirm or exclude the proposed long-term ^{237}Np self-radiation effect on these systems.

*3.3.3. Anomalous magnetic relaxation (creep) behavior in $NpO_2(acac)_2py$ (**2**)*

Low temperature magnetic-relaxation (creep) data of **2** below ∼9 K around which the onset of subtle ferromagnetism is observed in Fig. 4a are also remarkable. As shown in Fig. 6 for

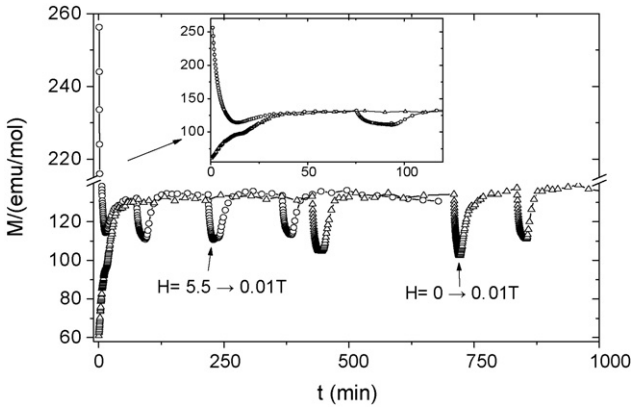

Fig. 6. Magnetic-relaxation (creep) data for $NpO_2(acac)_2py$ (**2**) at $T = 5$ K in prolonged time scale ($t = 0$–1000 min) ($w = 14$ mg, $M_W = 546.4$ g). Both data obtained for the ZFC ($H = 0 \rightarrow 0.01$ T) and RM ($H = 5.5 \rightarrow 0.01$ T) modes are shown. Inset shows the shorter-time data ($t = 0$–125 min) in extended scale.

$T = 5$ K, we observe here anomalously large magnetization (M) relaxation (creep) effect. As is clearly seen in the inset, both the ZFC ($H = 0 \rightarrow 0.01$ T) and RM ($H = 5.5 \rightarrow 0.01$ T) data exhibit very large M change within the initial 10–20 min. Almost a factor of two increase or decrease of M is observed for the ZFC or RM-mode, respectively, especially in the latter (RM) even exceeding the 'equilibrium' M ($=M_{eq}$) value. And this initial magnetic over-response is followed by a somewhat more gradual re-equilibration process back to the final 'equilibrium' state. Also as seen here, the ZFC and RM modes measured in sequence within the same run mostly converge more or less to the same M_e, if ever this shows discernable long-term fluctuation and drift. However, here again, such M_{eq} values are occasionally found to differ largely between the different runs. For example, though raw data are not shown here, in some extremely case at 2 K, the apparent M_{eq} value for one set of ZFC and RM ($H = 0$ and $5.5 \rightarrow 0.03$ T) is within the range of $\sim 800 \pm 50$ emu/mol at the final $H = 0.03$ T, while that of another set of ZFC and RM ($H = 0$ and $5.5 \rightarrow 1$ T) is much smaller $\sim 360 \pm 50$ emu/mol at the final $H = 1$ T. That is, the M_{eq} value at magnetic field ($H = 1$ T) about 33 times as large as that of the former ($H = 0.03$ T) is even less than one-half (1/2) of that of the former.

Together with the decisive fact that such anomalous creep behavior almost completely disappears above $T_C \sim 9$ K, it is already evident in the above examples that the most important direct origin (cause) of this anomalous creep behavior of **2** at low temperature is definitely the onset of subtle ferromagnetism inside the powder-interior bulk phase of **2**, i.e., the existence of bulk-interior low-T_C (<9 K) FM phase itself, rather than the above-clarified presence of minor high-T_C (>300 K) FM phase with its small saturation magnetization ΔM(ferro) = 47–53 emu/mol (Table 3 and Fig. 4b). For example, the initial creep M changes (ΔM_C (initial)) at 5 K shown in Fig. 6 ($H = 0$ or 5.5 T $\rightarrow 0.01$ T) are ~ 70 or ~ -130 emu/mol for the ZFC and RM modes, respectively, the both exceeding the above ΔM(ferro) of the minor high-T_C (>300 K) FM phase. Even more larger ΔM_C (initial) are commonly observed at lower-temperature runs, e.g., ΔM_C (initial) = ~ 200–~ -350 emu/mol for $H = 0$ or $5.5 \rightarrow 0.1$ T run at $T = 4.5$ K. Also, between the above-mentioned two relaxation runs at $T = 2$ K with their final $H = 0.03$ and 1 T, a very large difference in M_{eq} value ($\Delta M_{eq} = 800 - 360 = 440$ emu/mol) (even reversed in sign) is obtained. Obviously, all these values of ΔM_C (initial) and ΔM_{eq} are too large to be explained by the minor high-T_C (>300 K) FM contribution (ΔM(ferro) = 47–53 emu/mol), and hence convince us that the magnetization (M) of the bulk-interior low-T_C (<9 K) FM phase itself is here displaying such anomalous relaxation behavior. One other supporting evidence for this is that such anomalous creep behavior is not observed for **3**, in which the minor high-T_C (>300 K) FM phase is present either (though in smaller content (Table 3)), but the corresponding low T_C FC phase does not exist (Fig. 5) (or, if ever this exists at a little lower $T \sim 7$–8 K, this seems too subtle to be recognized as a ferromagnetic transition).

However, these do not at all mean that the presence of minor high-T_C (>300 K) FM phase has no connection with the occurrence of such anomalous low-temperature creep behavior of the major low-T_C (<∼9 K) FC phase of **2** including also its another peculiar feature mentioned just below. Rather inversely, from all the circumstantial evidences, it is inferred that the both are closely associated with each other in many aspects of these magnetic properties of **2**. That is, in our view, without such coexistence and interaction between the minor high-T_C (>300 K) and major low-T_C (<∼9 K) FM phases (a kind of proximity effect) it seems difficult to rationalize the occasional happening of the above-mentioned even-reversed anomalous run to run variation of M_{eq} at low temperature (<9 K) and that of the χ^{-1}–T plots at higher-temperature region up to 300 K for which one example is shown in Fig. 4a for the two set of $H = 0.01$ T data.

As also seen in Fig. 6, one other peculiar low-temperature magnetic feature of **2** (either not observed in **3**) is very large perturbation effect of the SQUID M measurement itself on the measured M_{eq}, i.e., the stepwise (about 10-times discrete) motion of the sample inside the differential-type SQUID magnetic flux detector (QD, MPMS). A perpetual or very short interval ($\Delta t = 0$ to several seconds) continuous or frequent M measurements of **2** is found to cause a spike-like ∼25–30% reduction of the measured M_{eq} (ΔM_{eq}(spike)) within ∼15–30 min, and the subsequent less-frequent measurements (by making Δt longer between the successive two measurements) smoothly returns the M to its apparent M_{eq} within almost the same or somewhat longer time scale. Even in case the former busy ($\Delta t = 0$ to several seconds) measurements are continued longer, the measured M value no more decreases, and the system only more slowly returns to the 'equilibrium'.

To eliminate the possibility that this peculiar magnetic response of **2** is due to some trivial technical problem of the present SQUID M measurement on this particular sample of **2** (Ø∼3 mm and several (2–4) mm long, embedded in a homogeneous cylindrical staycast sealant of Ø∼5 mm and ∼6 cm long), some additional experiments have been done. First we checked the effect of sample-scan length (l) from the minimum 3 cm to the maximum 6 cm to see the possible influence of in-homogeneity of the magnetic field (H) inside the sample chamber of the SQUID magnetometer. (The normally adopted is $l = 4$ cm for all our measurements.) Though this experiment showed some

enhancement of ΔM_{eq}(spike) at $l = 6$ cm compared to that at $l = 3$ cm, overall, such scan-length difference was found to have only minor effect well less than 5–10% difference in the measured ΔM_{eq}(spike)s, mostly masked by much larger run to run difference of such ΔM_{eq}(spike)s.

Secondly, we have performed the same creep measurements (at $l = 4$ m) at the same 5 K on two ceramics powder samples of almost the same shape and mass but with quite different magnetic characters: those are UO_2 (antiferromagnet (AF) with $T_N = 30.8$ K) and ZrN (type II superconductor with $T_C = 10.7$ K). In the former UO_2, we have definitively observed neither creep effect itself nor its AF–M alternation by such busy M measurement. On the other hand, For the latter ZrN (the upper critical field $H_{C2} = 0.3$ T [28a]), in the ZFC mode (e.g., $H = 0 \rightarrow 0.001$ T) the situation was analogous to the above UO_2 case, i.e., neither creep effect on its perfect diamagnetism in the Meissner state nor such perturbation effect on it were observed. While, in the RM mode ($H = 5.5 \rightarrow 0.001$ T) we do observed different kind of creep effect well-known as the so-called flux-creep phenomenon [28b] and also dissimilar perturbation effect that the more-busy M measurements tend to enhance the decrease of its apparently positive (paramagnetic) magnetization ($M > 0$) of the system, because this gives more-frequent external disturbance to its well-known thermodynamically meta-stable heterogeneous vortex state (the so-called mixed state) and hence enhances the flux-creep rate.

In analogy to the above flux-creep behavior in the mixed vortex state of type II superconductor ZrN and also to the so-called spin (or cluster) glass phenomenon, though the observed creep behavior here is more complex and quite different from such latter cases, this seems to be closely associated with the meta-stability and microscopic heterogeneity of the system either as in those latter cases, i.e., the coexistence of the minor high-T_C (>300 K) and major low-T_C (<∼9 K) FM phases and their mutual (possibly frustrated) magnetic interaction and competition, etc.

4. Conclusion

In this paper, we have presented an up-to-date summary mainly of our study on the unique low-D molecular magnetic properties of neptunyl ($O{=}(Np(V, VI){=}O)^{+1,+2}$; $5f^{2,1}$) complexes. On the basis of their structural and electronic features obtained from the XRD and Mössbauer data (Figs. 1 and 2, Table 1), the magnetic properties of oxo-neptunyl (+1) complexes are first discussed and summarized (Table 2). These clarify their basic identity as an Ising-type single neptunyl (+1)-molecule magnet with quenched magnetic moment from the free-ion value, and yet diverse character from a Curie-para- to ferro- and meta-magnets depending on their specific 0D to 2D CCB network structure with varied degree of 'nyl'-molecular distortion. Discussions are then extended to much-less studied neptunyl (+2) complexes for which such CCB is not generally formed, and here the results of our recent study on the three 0D (non-CCB) systems, an oxo-**1** and two N-substituted **2** and **3**, are presented (Tables 1 and 3, Figs. 3–6). While the oxo-**1**, together with the reported one other oxo-**4**, are confirmed to be Curie–Weiss paramagnets (Fig. 3), the N-substituted **2** and **3**, especially the former, are found to exhibit strikingly different magnetic features from the above oxo-neptunyls (+1, +2). Firstly, they showed strongly field (H)-dependent non-paramagnetic behavior up to 300 K (Figs. 4a and 5), and a plausible interpretation for this has been proposed based on the presence of minor high-T_C (>300 K) FM phase experimentally evidenced from the extensive M–H curve measurements (Fig. 4b). This minor high-T_C (>300 K) FM phase is supposed to be generated initially around the powder sample surface area by the chemical attack from the used epoxy-resin sealant and then steadily throughout by the radiation damage by the ^{237}Np α-decay. Further, **2** with largely distorted pentagonal-bipyramidal structure (CN = 7) different from the other three neptunyls (+2) (**1**, **3** and **4**) (CN = 8) was found to exhibit anomalous magnetic relaxation (creep) behavior at low temperature below ∼9 K around which its bulk phase shows subtle ferromagnetic order. This includes a peculiar initial magnetic over-response and its somewhat more-gradual drift back to a temporary apparent 'equilibrium' that differs tremendously from run to run influenced by some unknown history of the sample and/or unregulated experimental condition, and an unusually large perturbation effect of the SQUID-magnetization measurement itself on it, etc. Though the exact origin and mechanism for these anomalous magnetic features of **2** (and **3**) are not apparent at present (to elucidate them will need much-more future experiments), it seems that these anomalies best and symbolically illustrate the presence of largely meta-stable fluctuating magnetic (spin plus orbital) state both spatially and in time in **2** as a collective ensemble of an Ising-type individual neptunyl $(O{=}Np{=}O)^{+2}$ molecular magnets. Much remain for future study to elucidate these unique molecular magnetic properties of neptunyl (+1, +2) complexes and their N-substituted (and other) derivatives more in depth and further to explore this new area of actinide (5f) low-D molecular magnetism.

References

[1] N.N. Krot, D.N. Suglobov, Sov. Radiochem. (1990) 619.
[2] O. Kahn, Molecular Magnetism, Wiley–VCH, New York, 1993.
[3] P. Rabu, J. Phys. Chem. Solids, 65 (2004) 665 (Special Issue: Design, Characterization of Molecular-based Magnetic Materials), and see many papers in this issue.
[4] G.M. Kalvius, W. Potzel, J. Moser, F.J. Litterst, L. Asch, J. Zänkert, U. Potzel, A. Kratzer, M. Wunsch, J. Gal, S. Fredo, D. Dayan, M.P. Dariel, M. Boge, J. Chappert, J.C. Spirlet, U. Benedict, B.S. Dunlap, Physica B 130 (1985) 393.
[5] M. Zentkova, R. Göbl, M. Maryško, A. Zentko, Phys. Stat. Sol. (a) 172 (1999) R1.
[6] K.P. Mörtl, J.-P. Sutter, S. Golhen, L. Ouahab, O. Kahn, Inorg. Chem. 39 (2000) 1626.
[7] M. Ephritikhine, J. Chem. Soc., Dalton Trans. (2006) 2501.
[8] T. Nakamoto, M. Nakada, A. Nakamura, Y. Haga, Y. Onuki, Solid State Commun. 109 (1999) 77.
[9] T. Nakamoto, A. Nakamura, M. Saeki, Kotai Butsuri (Solid State Phys.) 34 (1999) 825 (in Japanese).
[10] T. Nakamoto, M. Nakada, A. Nakamura, Recent Research Developments in Inorganic Chemistry, vol. 2, Transworld Research Network, 2000, p. 145.
[11] T. Nakamoto, M. Nakada, A. Nakamura, Solid State Commun. 119 (2001) 523.

[12] T. Nakamoto, M. Nakada, A. Nakamura, J. Nucl. Sci. Technol. (Suppl. 3) (2002) 102.
[13] J. Wang, T. Kitazawa, M. Nakada, T. Yamashita, M. Takeda, Bull. Chem. Soc. Jpn. 75 (2002) 253.
[14] A. Nakamura, M. Nakada, T. Nakamoto, T. Kitazawa, M. Takeda, J. Phys. Soc. Jpn. (Suppl. 75) (2006) 146.
[15] D.M. Gruen, C.A. Hutchison Jr., Phys. Rev. 22 (1954) 385.
[16] (a) N.W. Alcock, M.M. Roberts, D. Brown, J. Chem. Soc., Dalton Trans. (1982) 33;
(b) N.W. Alcock, D.J. Flanders, M. Pennington, Acta Cryst. C 43 (1987) 1476;
(c) N.W. Alcock, D.J. Flanders, J. Chem. Soc., Dalton Trans. (1985) 1001.
[17] (a) M. Saeki, M. Nakada, N.M. Masaki, Z. Yoshida, K. Endo, Y. Minai, T. Yamashita, H. Muto, M. Magara, Hyperfine Interact. 92 (1994) 1177;
(b) M. Nakada, M. Saeki, N.M. Masaki, S. Tsutsui, J. Radioanal. Nucl. Chem. 232 (1998) 201;
(c) M. Nakada, N.M. Masaki, T. Yamashita, J. Nucl. Sci. Technol. (Suppl. 3) (2002) 426.
[18] H.H. Wickman, G.K. Wertheim, in: V.I. Goldanski, R.H. Herber (Eds.), Chemical Applications of Mössbauer Spectroscopy, Academic Press, New York, 1968 (Chapter 11).
[19] R.D. Shannon, Acta Cryst. A 32 (1976) 751.
[20] N.A. Bundantseva, G.B. Andreev, A.M. Fedoseev, M.Yu. Antipin, Radiochemistry 45 (2003) 303.
[21] E.R. Jones Jr., J.A. Stone, J. Chem. Phys. 56 (1972) 1343.
[22] M.S. Grigor'ev, I.A. Charushnikova, N.N. Krot, A.I. Yanovskii, Yu.T. Struchkov, Russ. J. Inorg. Chem. 41 (1996) 517.
[23] F. Nectoux, H. Abazli, J. Jove, A. Cousson, M. Pagès, M. Gasperin, G. Choppin, J. Less-Common Met. 97 (1984) 1.
[24] A. Cousson, S. Dabos, H. Abazli, F. Nectoux, M. Pagès, G. Choppin, J. Less-Common Met. 99 (1984) 233.
[25] T. Kawasaki, T. Kitazawa, T. Nishimura, M. Nakada, M. Saeki, Hyperfine Interact. (ICAME Proc. 2005), in press.
[26] (a) B.D. Dunlap, G.M. Kalvius, in: A.J. Freeman, J.B. Darby Jr. (Eds.), The Actinides: Electronic Structure and Related Properties, Academic Press, 1974, pp. 237–302;
(b) B.D. Dunlap, G.M. Kalvius, J. Phys. C4 (1979) 192.
[27] (a) T.E. Albrecht-Schmitt, P.M. Almond, R.E. Sykora, Inorg. Chem. 42 (2003) 3788;
(b) P.M. Almond, R.E. Sykora, S. Skanthakumar, L. Soderholm, T.E. Albrecht-Schmitt, Inorg. Chem. 43 (2004) 958;
(c) E. Jobiliong, Y. Oshima, J.S. Brooks, T.E. Albrecht-Schmitt, Solid State Commun. 132 (2004) 337;
(d) A.C. Bean, B.L. Scott, T.E. Albrecht-Schmitt, W. Runde, J. Solid State Chem. 177 (2004) 1346.
[28] (a) G. Burn, High-Temperature Superconductivity, An Introduction, Academic Press, Inc., Boston, 1992 (Chapter 2);
(b) G. Burn, High-Temperature Superconductivity, An Introduction, Academic Press, Inc., Boston, 1992 (Chapter 6).